3

Physics-Based Statistical Methods

Mott reached closure in his exploration of geometric fragmentation statistics early in his third internal report. In the remainder of this report he undertook a seminal investigation of the fragmentation of exploding shells, and developed a statistical theory of dynamic fragmentation elegant in its formulation and insightful in the physics explored. His theoretical effort has been noted in numerous subsequent studies in dynamic fragmentation but has received little in-depth study. Consequently, the fragmentation theory of Mott now over 60 years in the literature has been neither validated nor refuted. Efforts in the present section attempt to assess and broaden the physical principles of dynamic fragmentation first proposed by Mott. The efforts go beyond the initial analysis of Mott, however, both in the range of fracture processes, as well as in the analytic development.

3.1 Statistical Theory of Mott

The dynamic fracture analysis pursued by Mott is decidedly one-dimensional. It is best visualized as that of a uniformly stretching rod or expanding ring such as illustrated in Fig. 3.1. The model can be usefully abstracted to fragmentation applications, such as a rapidly expanding cylinder in which the circumferential stretching rate substantially exceeds the axial, or a one-dimensional spall event within a body experiencing increasing tension within a region of uniform axial velocity gradient. Here, for clarity, the model exploration will focus on a stretching filament of material of unit cross section as depicted by the expanding ring in Fig. 3.1. Prior to fracture, the body is uniformly stretched to an axial strain ε which is increasing at a constant strain rate $\dot{\varepsilon}$.

Mott considered the body to be rigid perfectly plastic and straining in tension under a constant flow stress Y. The Mott kinematic conditions will be referred to as plastic fracture. Tensile loading in which the body remains elastic up to the point of fracture will also be considered (elastic fracture). Here

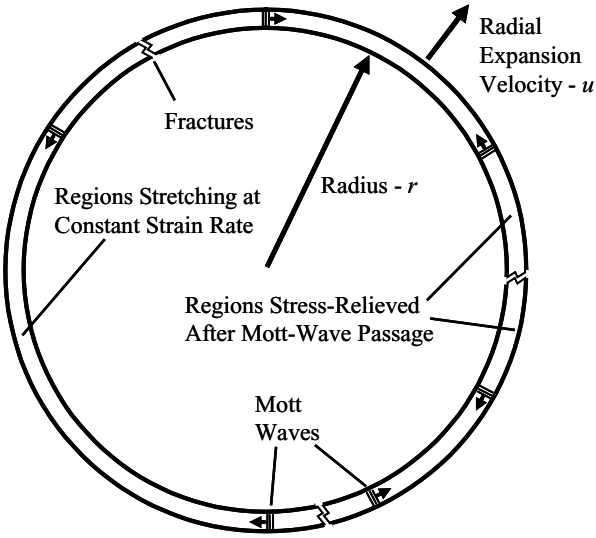

Fig. 3.1. The one-dimensional Mott problem. A one-dimensional ring of material undergoes outward expansion at constant velocity, u. Prior to fracture response of the body is uniform tensile stretching at a strain rate $\dot{\varepsilon} = u/r$. Instantaneous fracture occurs at random sites and waves originate at points of fracture which propagate at finite speeds, relieving tensile stress and further stretching. Strain-dependent fracture continues only in regions not yet encompasses by the stress-relieved waves

tensile stress is related to strain and strain rate according to $\sigma = E\varepsilon = E\dot{\varepsilon}t$ where E is the appropriate elastic modulus.

At onset of breakup fractures are considered to occur at random in both time (or equivalently strain) and in spatial location on the stretching body as illustrated in Fig. 3.1. Following Mott it is assumed that fractures occur instantaneously relieving the tensile stress at the point of fracture to zero. Thus fracture resistance at the point of breakage and corresponding fracture energy during the breakage process is ignored.

Mott argued that the fracture energy was not significant. Rather, he proposed that the statistical nature of the fracture process determined both the characteristic fragment size, as well as the distribution in fragment sizes.

Mott's assumption of both instantaneous fracture and the insignificance of fracture energy can, and should, be examined further. This issue will be investigated in some detail in a later section.

Mott used observations of fracture in notched-bar specimens of steels to support the theoretical approach. He noted that the reduction in the cross-sectional area (the strain) before fracture was not the same from test to test. Scatter in the strain to fracture of a few percent over a number of tests was observed. He then proposed that strain to fracture was a random variable in

the stretching body, and that fracture when the circumferential strain achieved some critical level was governed by probabilistic causes.

Following fracture at a point, waves propagate away from the fracture relieving the tensile stress and subsequent stretching within the regions encompassed by the waves. For plastic fracture, in which waves are propagating into media stretching plastically at a constant flow stress Y these waves are diffusive (Mott waves) and the distance traveled depends on time and physical properties according to,

$$x = \sqrt{2Yt/\rho\dot{\varepsilon}} \; . \tag{3.1}$$

If fracture is elastic, release waves propagate according to,

$$x = \sqrt{E/\rho}t \; , \tag{3.2}$$

where $c = \sqrt{E/\rho}$ is the elastic wave speed.

Fracture physics in either the plastic or the elastic model is governed by the competition of waves of release emanating from existing fractures, with continuing fracture occurring within regions of the body not yet subsumed by these waves.

3.2 Mott Wave Propagation

Equation (3.1) describes the time-dependent propagation of tensile stress release from points of fracture, and is representative of the insightful physics introduced by Mott in pursuing an understanding of the dynamic fracture process.

3.2.1 Mott Rigid Plastic Solution

To pursue his analysis of the distribution of the fracture spacing resulting in the dynamic fracture of an expanding cylindrical shell, it was necessary to establish the speed at which waves, signaling the drop in tensile stress, propagated outward from points of fracture. Accordingly, Mott considered a one-dimensional rod of unit cross section stretching plastically under a tensile stress Y and uniformly at a constant stretching rate, $\dot{\varepsilon}$. Fracture was initiated by setting the tensile stress to zero at time $t = 0$ at some Lagrangian position, say $h = 0$. Regions of the rod experiencing tensile stress less than Y were considered rigid. Mott then realized that a boundary (herein called a Mott wave) separated rod material stretching uniformly at stress Y in front of the boundary from rigid material moving at the same uniform velocity behind the boundary. This boundary (Mott wave) propagates away from the point of fracture at $h = 0$. Features of the stress and velocity associated with the Mott wave at some time $t > 0$ are illustrated in Fig. 3.2. Location of the Mott wave is identified by $x(t)$, while crack opening displacement is given by $y(t)$. The velocity field is then,

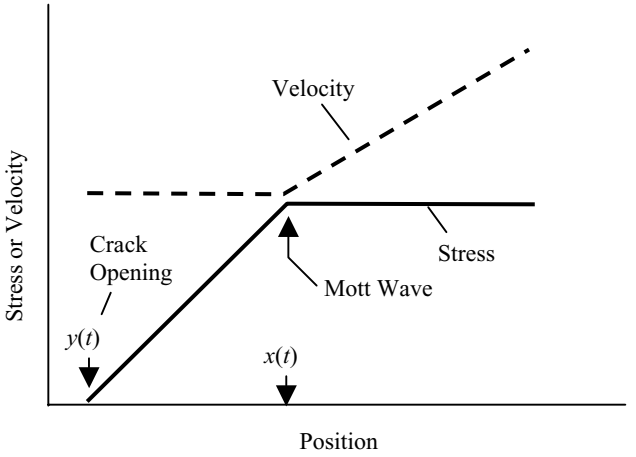

Fig. 3.2. Stress and velocity field at time t after fracture at position $h = 0$ drops tensile stress from Y to zero

$$u\,(h,t) = \begin{cases} \dot{\varepsilon} x\,(t) & 0 \le h < x\,(t) \\ \dot{\varepsilon} h & x\,(t) \le h \le h_o \end{cases} , \tag{3.3}$$

where, h_o is some arbitrary distance.

The corresponding stress field is equally apparent. The total momentum of the rod within the region $0 \le h \le h_o$ is just,

$$\rho\dot{\varepsilon}x^2 + \int_x^{h_o} \rho\dot{\varepsilon}h dh = \frac{1}{2}\rho\dot{\varepsilon}(x^2 + h_o^2)\,. \tag{3.4}$$

Equating the time rate of change of momentum to the imbalance in tensile stress yields the differential equation,

$$\rho\dot{\varepsilon}x\frac{dx}{dt} = Y\,, \tag{3.5}$$

for the position $x(t)$ of the Mott wave at time t. Integration readily yields,

$$x\,(t) = \sqrt{\frac{2Yt}{\rho\dot{\varepsilon}}}\,. \tag{3.6}$$

Thus, fractures occurring in the stretching body lead to the propagation of waves, away from these points of fracture, which unload the tensile stress. The time dependent motions of these Mott waves are governed by both material properties and kinematic conditions according to the relation above. Within regions subsumed by Mott waves, further fracture will not occur. Subsequent fracture will only occur in regions, not yet reached by the unloading Mott waves, which continue to stretch unimpeded at a rate $\dot{\varepsilon}$ and flow stress Y.

Mott recognized that excessively high velocities of the interface $x(t)$, at early times, was a consequence of the rigid-plastic assumption and inconsistent with a more rigorous elastic-plastic treatment of the problem. He acknowledges an analysis due to E. H. Lee, which was published some years later [Lee, 1967]. Lee considered the same initial and boundary conditions posed by Mott, but treated material response behind the interface as elastic. It is shown that the initial drop in stress from $\sigma = Y$ to $\sigma = 0$ at the origin $h = 0$ propagates as a decaying shock discontinuity in stress and particle velocity at an elastic wave speed c. This shock discontinuity decays to zero at a distance of,

$$h = \frac{2Y}{\rho c \dot{\varepsilon}} = \lambda \,, \tag{3.7}$$

and at a time of,

$$\tau = \lambda / c \,. \tag{3.8}$$

Subsequent reflected elastic waves and the interface $x(t)$ are acceleration discontinuities (discontinuities in the slopes of stress and particle velocities). Continued solution reveals that the interface $x(t)$ is a polygon in the h vs. t domain with vertices,

$$h = n\lambda \,, \quad t = n^2 \lambda / c \,, \quad n = 1, 2, 3, \ldots \tag{3.9}$$

where each segment propagates at a velocity of,

$$c_n = \frac{c}{2n - 1} \,. \tag{3.10}$$

The rigid-plastic solution of Mott (1947) and the elastic-plastic solution of Lee (1967) are compared in Fig. 3.3. The former is found to envelop the elastic-plastic solution touching at the vertices. Within several characteristic distances λ the rigid-plastic solution is found to be a very good approximation to both the position of the interface, and to the stress and velocity field behind the interface.

3.2.2 The Diffusion Solution

It is the simplicity of Mott's analysis which so vividly reveals the underlying physics. It is readily apparent that Mott's solution is intended to apply at the point at which hardening in the stretching rod saturates, and the tension versus strain loses its hyperbolic character. At this point of stationary tension, the governing equations become parabolic, and the diffusive nature implicit in the motion of the Mott wave is expected.

The diffusive character of the stress release process can in fact be readily demonstrated by writing the linear diffusion relation,

$$\frac{\partial^2 \sigma}{\partial h^2} - \frac{1}{\kappa} \frac{\partial \sigma}{\partial t} = 0 \,, \tag{3.11}$$

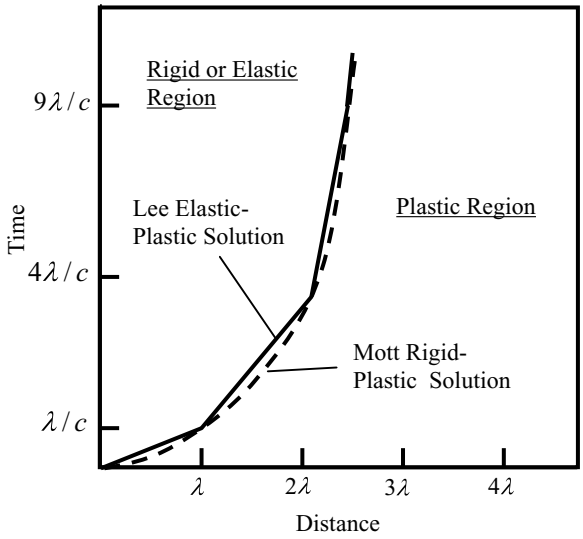

Fig. 3.3. Comparisons of interface $x(t)$ separating plastic region and rigid plastic region according to solutions of Mott (1947) and Lee (1967)

with the diffusion constant,

$$\kappa = Y/2\rho\dot{\varepsilon} \ . \tag{3.12}$$

Consider the same problem treated by Mott in which fracture at $t = 0$ and $h = 0$ instantly decreases the tensile stress from $\sigma = Y$ to $\sigma = 0$. This classic solution [e.g., Matthews and Walker, 1964] can be immediately written down for the stress,

$$\sigma/Y = erf\,(\xi) \ , \tag{3.13}$$

and the velocity,

$$\frac{u}{\dot{\varepsilon}\sqrt{4\kappa t}} = \sqrt{\frac{4}{\pi}}\exp\left(-\xi^2\right) + 2\xi erf\,(\xi) - \xi \ . \tag{3.14}$$

In (3.13) and (3.14) the similarity parameter,

$$\xi = h/\sqrt{4\kappa t} \ , \tag{3.15}$$

has been introduced. The present diffusion equation solution and the rigid-plastic solution of Mott are compared in Fig. 3.4.

The rigid-plastic solution of Mott, the elastic-plastic solution of Lee, and the solution to the diffusion equation are, of course, only models of the actual processes of fracture and stress unloading occurring in the rupture of a rapidly stretching ductile shell. Which model most accurately depicts reality probably cannot be answered. All, however, reveal physics of the fracture process and point to the decidedly diffusive nature of stress wave propagation.

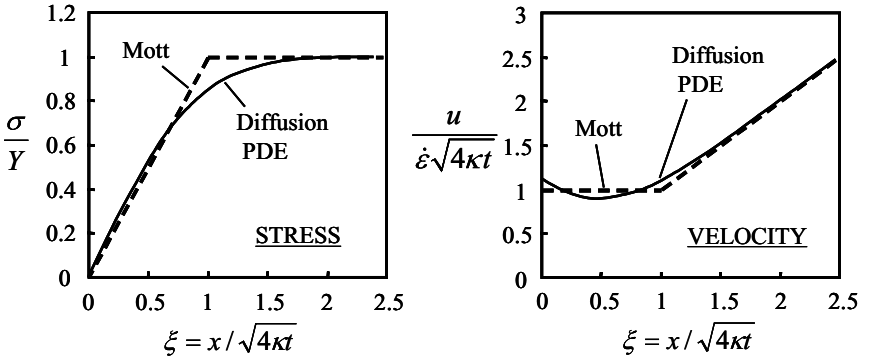

Fig. 3.4. Comparisons of solutions for Mott's rigid-plastic model and a linear stress-diffusion model of fracture in a stretching plastic rod

3.2.3 Fracture Energy Solution

One further extension of the fracture wave analysis developed by Mott is of interest. Mott was convinced at the time of development of the rigid-plastic fracture release wave solution that energy dissipated at the point of fracture was inconsequential and could be ignored. Hence, the assumption of instantaneous stress drop at the point and time of fracture was inherently sensible. The solution method is readily amenable to considerations of fracture when the fracture energy is not inconsequential, [Grady et al., 1984; Kipp and Grady, 1985].

From (3.4), which equates the rate of change of momentum of the circumferential strip of stretching case material $0 \leq h \leq h_o$, adjacent to a fracture initiated at $h = 0$ and at time $t = 0$, to the misbalance in tensile stress at opposite ends of that strip, obtain,

$$\rho\dot{\varepsilon}x\frac{dx}{dt} = \sigma\left(h_o\right) - \sigma\left(0\right). \tag{3.16}$$

The boundary condition in Mott's solution method sets $\sigma(0) = 0$ at $t = 0$ corresponding to instantaneous stress release at the moment of fracture. It is reasonable, however, to consider a model in which the tensile stress is reduced gradually over time from $\sigma(0) = Y$ to $\sigma(0) = 0$ as the crack opens. This model would replicate a fracture resisting crack opening and thus, dissipate energy in the crack-opening process. As illustrated in Fig. 3.5, a coordinate $y(t)$ identifies the crack-open displacement, while $x(t)$ determines the position of the rigid-plastic boundary. A fracture resistance is proposed in which the boundary tensile stress reduces linearly to zero at $y = y_c$. (Other possible models for the boundary resistance are considered in Chap. 4.) An energy of fracture is then given by $\Gamma = Yy_c/2$, the area under the stress-displacement curve. The concepts are quite analogous to crack-opening-displacement models of Dugdale (1960) and Barenblatt (1962) in the treatment of quasistatic fracture

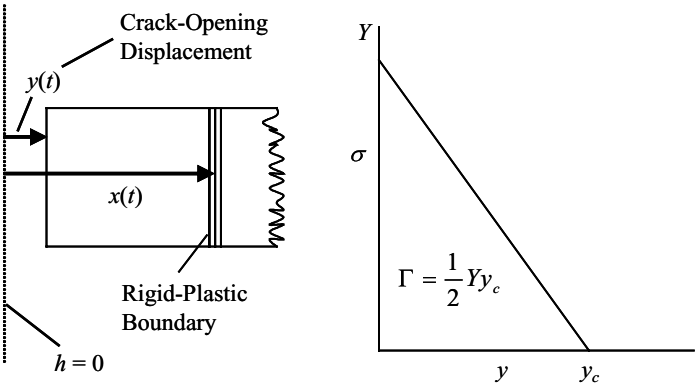

Fig. 3.5. The sketch on the left illustrates crack-opening displacement y due to motion of the rigid section of the strip. On the right the resisting tensile stress as a function of crack-opening displacement is shown which dissipates an energy Γ when displacement achieves a value y_c

resistance. Equation (3.16) then gives the momentum balance relation,

$$\rho\dot{\varepsilon}x\frac{dx}{dt} = \frac{Y^2}{2\Gamma}y \,, \tag{3.17}$$

while motion of the crack-opening displacement provides,

$$\frac{dy}{dt} = \dot{\varepsilon}x \,. \tag{3.18}$$

The coupled (3.17) and (3.18) are readily solved yielding,

$$x\,(t) = \frac{1}{12}\frac{Y^2}{\rho\Gamma}t^2 \,, \tag{3.19}$$

for motion of the rigid-plastic boundary during the crack-opening displacement $0 \le y \le y_c$. The solution for crack-opening displacement is in turn given by,

$$y\,(t) = \frac{1}{36}\frac{\dot{\varepsilon}Y^2}{\rho\Gamma}t^3 \,. \tag{3.20}$$

When y exceeds y_c (completion of fracture) the original solution of Mott applies.

Setting $y = y_c$ in (3.20) and using the expression for fracture energy, $\Gamma = Yy_c/2$, the time t_f at which fracture is complete can be calculated,

$$t_f = \left(\frac{72\rho\Gamma^2}{Y^3\dot{\varepsilon}}\right)^{1/3} \,. \tag{3.21}$$

Correspondingly, the distance x_f traveled by the rigid-plastic boundary during the time of fracture completion from (3.19) is,

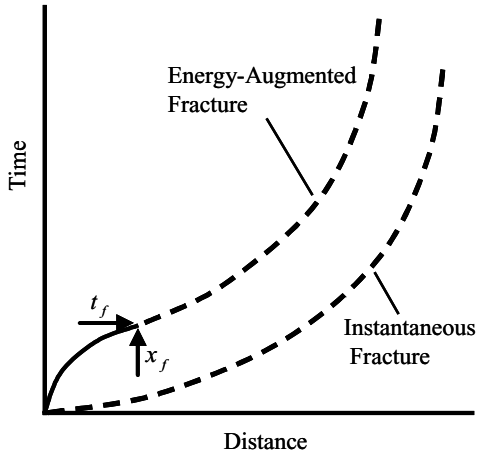

Fig. 3.6. Motion of the rigid-plastic boundary with a resisting fracture energy model is compared with original instantaneous-fracture solution of Mott

$$x_f = \left(\frac{3\Gamma}{\rho\dot{\varepsilon}^2}\right)^{1/3} . \tag{3.22}$$

The motion of the rigid-plastic boundary with the present resisting fracture energy model is compared with Mott's original instantaneous-fracture solution in Fig. 3.6. Equation (3.19) governs the motion until the fracture time t_f at a distance x_f is achieved. Subsequent motion is governed by the same free-boundary conditions as that of instantaneous fracture. The principal effect is to cause a delay in the boundary motion compared to the motion of instantaneous fracture.

It is apparent that if two fractures initiate within a time t_f and with spacing between them of less than $2x_f$ they will interfere with each other before the fracture growth process is complete. Such interactions have been studied and have shown under certain criteria that one or the other of the two fractures will arrest growth and not complete the fracture process [Kipp and Grady, 1985]. Out of this study a nominal fracture spacing of twice x_f or,

$$x_o = \left(\frac{24\Gamma}{\rho\dot{\varepsilon}^2}\right)^{1/3} , \tag{3.23}$$

has been proposed when conditions in the fracture process favor sufficient fracture initiation sites such that fracture interaction and competition processes governed by energy requirements determines the breakup intensity.

Thus, like Lee's elastic-plastic solution places a lower bound on the distance of interface propagation before Mott's rigid-plastic solution is adequate, the present analysis places a lower bound on fracture spacing governing Mott's instantaneous fracture assumption.

The above analysis, of course, opens further questions. What, for example, would be the effect on the calculated fracture properties if crack-opening resistance models other than linear softening were pursued? Also, to what extent are fracture properties sensitive to the scale of initial perturbations responsible for fracture onset? These extended issues detract, however, from the pursuit of Mott's fracture theory, but have been included in a section of the next chapter.

3.3 Statistical Fundamentals

Mott proposed that the occurrence of fracture in a stretching body is governed by a fracture frequency probability function $\lambda(\varepsilon)$ of the strain ε. The expression $\lambda(\varepsilon)d\varepsilon dl$ is the chance that a fracture will occur in a length dl at a strain ε within an interval $d\varepsilon$. Dimensionally it can be considered the random frequency of fracture per unit strain and length of the stretching body. It is useful for both later developments, and for the present conceptualization to consider an expanding ring composed of a large number N_o of equal length segments. Imagine further each of these segments stretching independently, but at the same rate. For the moment it is also convenient to consider segments of unit initial length. Then at a strain ε,

$$\frac{dN}{N} = -\lambda\left(\varepsilon\right) d\varepsilon \ , \tag{3.24}$$

is the fraction of the surviving segments N that fracture as the strain is increased from ε to $\varepsilon + d\varepsilon$. Equation (3.24) is integrated to provide the surviving number of segments as a function of strain,

$$N = N_o e^{-\int \lambda(\varepsilon) d\varepsilon} \ . \tag{3.25}$$

Equation (3.25) readily provides the cumulative probability distribution for fracture within a body of unity length at or before a strain ε is achieved,

$$F\left(\varepsilon\right) = 1 - e^{-\int \lambda(\varepsilon) d\varepsilon} \ . \tag{3.26}$$

The probability of a unit length surviving when strain ε is achieved is, of course,

$$1 - F\left(\varepsilon\right) = e^{-\int \lambda(\varepsilon) d\varepsilon} \ . \tag{3.27}$$

The complementary cumulative probability density function for a unit length surviving to strain ε and fracturing within the subsequent unit strain interval is,

$$f\left(\varepsilon\right) = \frac{dF\left(\varepsilon\right)}{d\varepsilon} = \lambda\left(\varepsilon\right) e^{-\int \lambda(\varepsilon) d\varepsilon} = \left(1 - F\right) \lambda\left(\varepsilon\right) \ . \tag{3.28}$$

In the statistical theory of reliability or life testing the function $\lambda(\varepsilon)$ is commonly known as the hazard function or the conditional failure (mortality)

function [Hahn and Shapiro, 1967] and is more generally identified as $h(\varepsilon)$ in later analysis. Typically time rather than strain is the random variable. However, in the present development time and strain are related through a constant strain rate $\varepsilon = \dot{\varepsilon}t$, and the two random variables are synonymous.

Mott (1943) proposed three functional forms for the fracture frequency function $\lambda(\varepsilon)$. They are

$$\lambda(\varepsilon) = \lambda_o, \quad \text{a constant} , \tag{3.29}$$

$$\lambda(\varepsilon) = \frac{n}{\sigma}\left(\frac{\varepsilon}{\sigma}\right)^{n-1}, \ (n \geq 1) , \tag{3.30}$$

$$\lambda(\varepsilon) = Ae^{\gamma\varepsilon} . \tag{3.31}$$

The first is, of course, a special case of the second power law representation for $n = 1$ leading to a constant or uniform fracture frequency. Mott suggested that the first two expressions could be zero up to some $\varepsilon = \varepsilon_o$ taking their functional representation thereafter. This is not of consequence. Much of Mott's attention attended to the later exponential representation for $\lambda(\varepsilon)$ in (3.31).

The three fracture frequency functions are illustrated in Fig. 3.7. Although, diversely different in this representation, it was shown by Mott that their consequences on fragment size and distribution were not dramatically different.

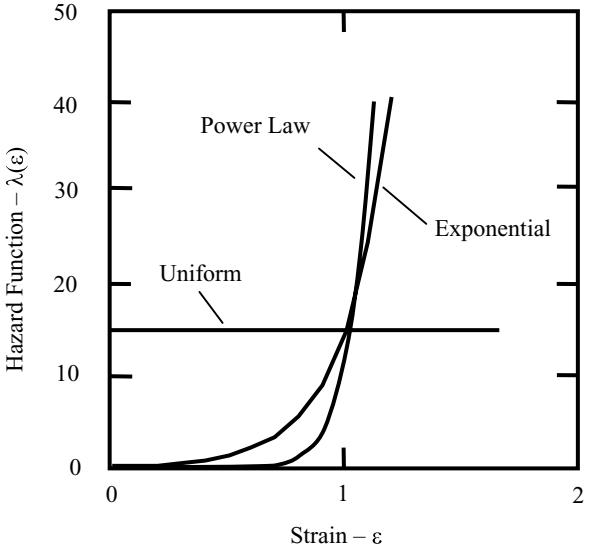

Fig. 3.7. The fracture frequency hazard functions for strain-to-fracture proposed by Mott are compared. The parameters are for the uniform function, $\lambda_o = 15$; the power-law function, $\sigma = 1, n = 12$: and the exponential function, $A = 0.1, \gamma = 5$

Their functional forms have been explored extensively in treatise on statistics [e.g., Hahn and Shapiro, 1967]. The first constant hazard function leads to the familiar exponential probability distribution used, for example, in radioactive decay. The second power-law hazard function leads to the Weibull distribution commonly used in the breaking strength of materials. This distribution reduces to the exponential distribution for $n = 1$ and the Rayleigh distribution for $n = 2$. The third hazard function is a form of asymptotic or extreme-value probability distribution and leads to the Gumbel extreme value distribution [Hahn and Shapiro, 1967].

We will principally pursue the consequences of a power law function and the resulting Weibull distribution for the statistical fragmentation of a one-dimensional stretching body. It has, in the intervening years, become the common statistical representation for strength of solids. Doremus (1983) has pointed out, however, that in spite of popularity of the Weibull distribution, the normal distribution, and the Gumbel distribution, can in some applications better characterize strength data in solids. He points out that Weibull selected the power law form for mathematical convenience and that there was no theoretical basis. There are important differences between the two distributions for the present fragmentation application, which will be pointed out after details of the distributions are discussed.

The Weibull probability density function for fracture within a unit circumferential length of the cylinder is,

$$f(\varepsilon) = \frac{n}{\sigma}\left(\frac{\varepsilon}{\sigma}\right)^{n-1} e^{-(\varepsilon/\sigma)^n} , \tag{3.32}$$

while the cumulative distribution function is,

$$F(\varepsilon) = 1 - e^{-(\varepsilon/\sigma)^n} . \tag{3.33}$$

Shape and scale parameters of the distributions are n and σ, respectively. Both probability-density and cumulative probability distribution functions are shown in Fig. 3.8. Curves illustrate the tendency for the fracture to center about a fixed strain to failure with increasing shape parameter n. The expected value for strain to failure is given by,

$$\sigma\, \Gamma\left(1 + \frac{1}{n}\right) , \tag{3.34}$$

where $\Gamma(\ )$ is the gamma function. The standard deviation about the mean is provided by,

$$\sigma\left[\Gamma\left(1+\frac{2}{n}\right) - \left(\Gamma\left(1+\frac{1}{n}\right)\right)^2\right]^{1/2} \cong 1.28\frac{\sigma}{n} . \tag{3.35}$$

The asymptotic limit as $n \to \infty$ for the standard deviation is shown in (3.35) and is a reasonable estimate over much of the range of n. The functional

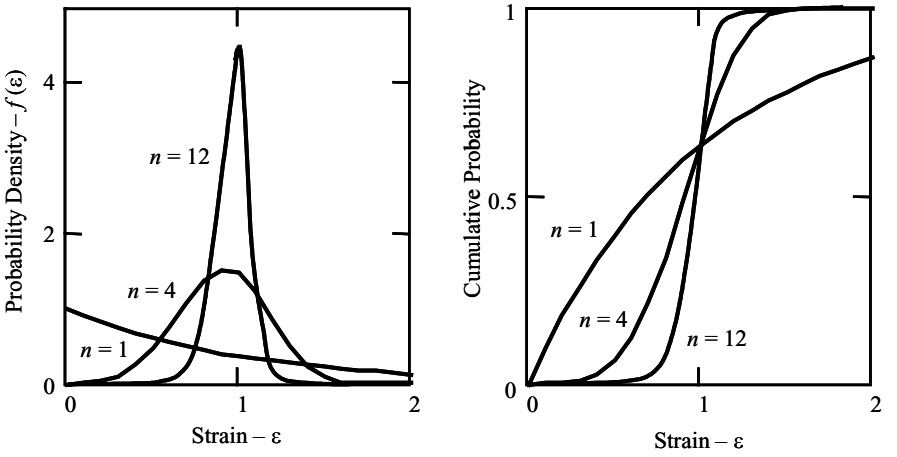

Fig. 3.8. Probability density and cumulative probability distributions for power-law fracture frequency function (Weibull distribution) with selected values of shape parameter n. The scale parameter is $\sigma = 1$

form of these statistical properties for the Weibull distribution is illustrated in Fig. 3.9.

For a body of arbitrary length l the hazard function $\lambda(\varepsilon)$ is replaced by $l\lambda(\varepsilon)$ in previous relations. It is readily shown that σ in (3.34) and (3.35) is

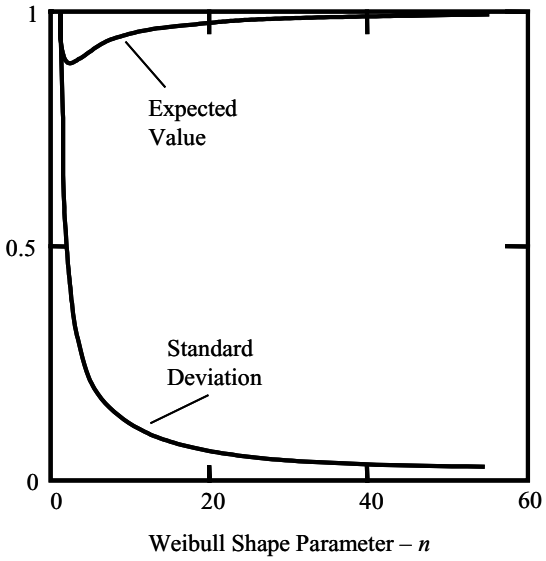

Fig. 3.9. Expected value and standard deviation for strain-to-fracture with increasing values of the Weibull shape parameter n. The scale parameter is $\sigma = 1$

then replaced by $\sigma/l^{1/n}$ illustrating the size dependence of fracture strength common to Weibull statistics.

With reasonably high values of n the power-law hazard function and Weibull distribution quite adequately describe the several percent scatter in failure strain observed in metal tensile specimens. This analytic distribution thus provides a reasonable statistical representation for describing the multiple fragmentation process in rapidly stretching bodies such as the expanding ring illustrated in Fig. 3.1.

In contrast, the strain-to-fracture exponential hazard function $\lambda(\varepsilon) = A\exp(\gamma\varepsilon)$ and the resulting fracture distribution function chosen by Mott for study is, like the power law hazard function and Weibull distribution function, a form of extreme value distribution. More specifically it is commonly known as the Gumbel extreme value distribution [Hahn and Shapiro, 1967]. Characteristics of the distribution are more transparent rewriting the hazard function in the form,

$$\lambda(\varepsilon) = \frac{1}{\sigma} e^{(\varepsilon-\mu)/\sigma} , \tag{3.36}$$

where the correspondence $\sigma = 1/\gamma$ and $(1/\sigma)\exp(-\mu/\sigma) = A$ is made with the relation of Mott. The probability density function for strain-to-fracture is then,

$$f(\varepsilon) = \frac{1}{\sigma}\exp\left(\frac{1}{\sigma}(\varepsilon-\mu) - e^{(1/\sigma)(\varepsilon-\mu)}\right) . \tag{3.37}$$

Both hazard function and probability density function for Gumbel distribution are illustrated in Fig. 3.10. The parameter μ is seen to be the distribution mode and location parameter, while the expected strain to fracture is,

$$\mu - n_e\sigma , \tag{3.38}$$

where $n_e = 0.577$ is the Euler number. The distribution standard deviation is,

$$1.283\sigma . \tag{3.39}$$

Thus, not unlike the Weibull distribution, as σ approaches zero the expected value approaches the mode μ and the distribution converges to a delta function.

It is important at this juncture to point out a very significant difference between the Gumbel extreme value distribution (selected by Mott for application to fragmentation statistics) and the Weibull distribution. Whereas the latter has both a distribution scale and shape parameter, the Gumbel distribution parameters determine only the scale and the location of the distribution but are lacking a shape parameter. This difference will be shown to have an important influence on the theoretically predicted dependence of fragment size on the strain rate. The Gumbel distribution will yield a unique inverse first power dependence on strain rate. Over physically reasonable values of the shape parameter n the Weibull distribution predicts a strain rate dependence

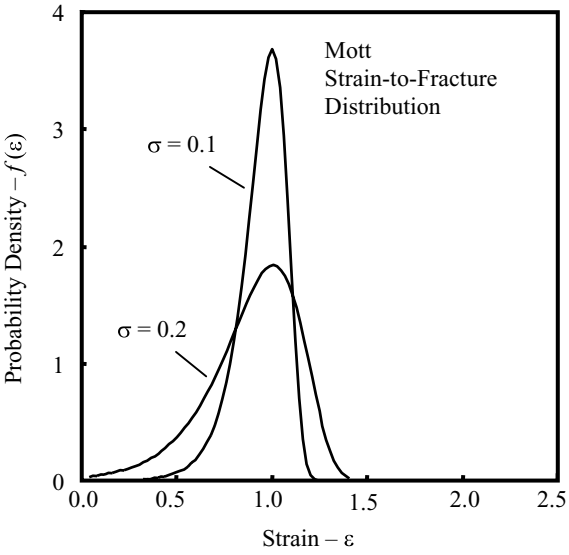

Fig. 3.10. Illustrates the Mott strain-to-failure distribution (Gumbel extreme value distribution) with distribution location parameter $\mu = 1$ and several values of the scale parameter σ

ranging between an inverse first power and an inverse two-thirds power. Mott commented on these differences but did not provide strong justification for selection of the Gumbel distribution.

3.4 The Mott Distribution

The physical and statistical principles just outlined were then used by Mott to determine a distribution in fragment lengths (or fracture spacing) resulting from the plastic fracture of the expanding Mott ring. It should be emphasized that this one-dimensional distribution bears no relationship to the earlier two-dimensional Mott distribution arrived at intuitively by Mott and Linfoot from Lineau's theoretical efforts.

Mott noted that he was not able to develop an analytic solution and proceeded with a graphical method which is described below. It seems likely that with a modest amount of additional time to reflect on his theory Mott would have developed an analytic solution, which was his nature. It is interesting that nearly concurrently other workers [Johnson and Mehl, 1939] were pursuing transformation reaction kinetics in metals and developed analytic tools ideally suited to Mott's statistical fragmentation theory. This sensible extension to the Mott development will also be described here.

The graphical solution to the statistical fragment size distribution derived by Mott proceeds as follows: A parameter D is defined, which is a function of

time t (or strain) such that $0 \leq D(t) \leq 1$. At any time $D(t)$ is the fraction of the stretching body (Fig. 3.1) which has been subsumed by the Mott release wavelets propagating from the points of fracture. Since further fractures are assumed to occur only in the fraction of the body not yet encompassed by these release wavelets $1 - D$, clearly the probable number of fractures which will appear in the time increment t to $t + dt$ is,

$$dN = (1 - D)\,\lambda(\dot{\varepsilon}t)\,\dot{\varepsilon}dt\ . \tag{3.40}$$

As previously pointed out, Mott chose to explore the fracture frequency relation $\lambda(\dot{\varepsilon}t) = A\exp(\gamma\dot{\varepsilon}t)$.

The release fraction $D(t)$ of the plastic stretching body considered by Mott is determined by the collective Mott waves emanating from fractures initiating prior to time t. Each Mott wave propagates according to,

$$x_i = \sqrt{2Y/\rho\dot{\varepsilon}}\,(t - t_i)^{1/2}\ , \tag{3.41}$$

where t_i is the initiation time of the ith fracture. Introducing a dimensionless time through,

$$\xi = \gamma\varepsilon = \gamma\dot{\varepsilon}t\ , \tag{3.42}$$

Equation (3.41) becomes,

$$x_i = \sqrt{2Y/\rho\dot{\varepsilon}^2\gamma}\,(\xi - \xi_i)^{1/2}\ , \tag{3.43}$$

where Mott recognizes the radical expression on the right of (3.43) as the normalizing length scale (proportional to the average fragment length) for the distribution in fragment lengths.

To determine the fragment distribution Mott worked with (3.40) and (3.43). A graphical solution was carried out whereby he introduced fractures at random at successive times determined by (3.40), and computed the collective release fraction of the body $D(t)$ with (3.43). Performing this task a number of times provided a credible histogram of the distribution in fragment lengths. The resulting distribution obtained by Mott as both a density distribution and a complementary cumulative distribution is shown in Fig. 3.11. The normalizing length, L_o is that identified in (3.43). From the graphical distribution Mott noted that the average fragment size was about 1.5 L_o. Again this distribution bears no relation to the Mott distribution inferred by Mott and Linfoot from Lineau's theoretical efforts, and that is commonly used to represent munitions fragmentation data.

This author is aware of only one effort to duplicate the statistical size distribution analysis performed by Mott. Wesenberg and Sagartz (1977) performed fragmentation experiments through magnetic inductive expansion of aluminum cylindrical shells (see Chap. 8). Using computer methods and an appropriate random number generator, they produced fragment size distributions by solving the same pair of equations as Mott (3.40) and (3.43). Distribution results were compared with their fragmentation data.

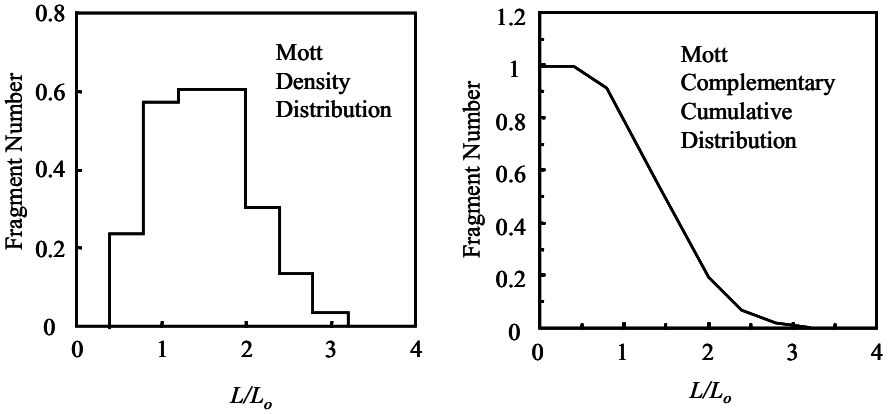

Fig. 3.11. The fractional number density distribution (*left*) and fractional complementary cumulative number distribution (*right*) determined by Mott (1947) for the fragmentation of a uniformly stretching plastic body. Normalizing length scale L_o is identified in the text

Wesenberg and Sagartz displayed their calculated distributions as the average of the individual results of 10 rings, 100 rings, and 1000 rings, respectively, and concluded that a reasonably large number of calculations was required to achieve sensible convergence. Their distribution resulting from the average of 1000 rings is shown in Fig. 3.12 and compared with the distribution of Mott.

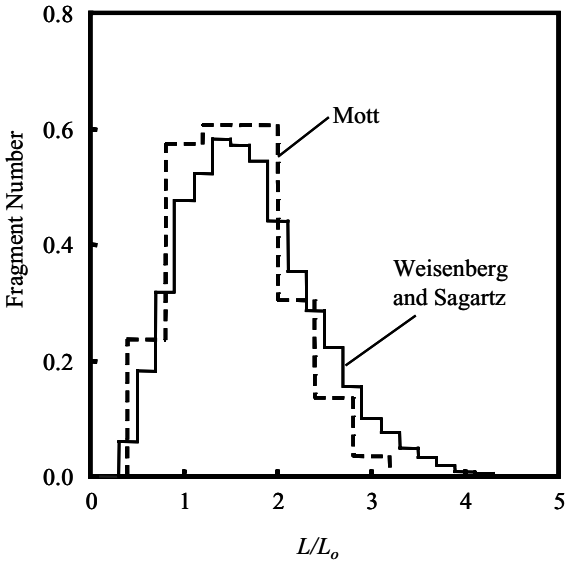

Fig. 3.12. Comparisons of fragment distributions calculated by Mott (1947) and by Weisenberg and Sagartz (1977)

3.5 Dynamic Fracture as a Statistical Transformation Process

In the present and subsequent subsections the essential ideas proposed by Mott on statistical fracture and fragmentation will be pursued further. The analytic statistical methods to be described will not necessarily provide improved predictive capabilities. They will, however, provide alternative points of view and provide analytic relations which are potentially amenable to generalization to more complex fragmentation problems. These methods also help to clarify scaling features in the predicted fragment sizes and distributions.

The processes of dynamic fracture and fragmentation involve spatially and temporally random nucleation and growth of fractures that have similarities to other nucleation and growth phenomena (melting, recrystallization, detonation reaction, etc.). In fracture, as in some of the other phenomena, nucleation and growth of a single fracture can be treated in substantial detail. It is the impingement or influence of one fracture, or region of growth, on others which compounds the complexity of the total nucleation and growth process.

To treat problems of nucleation and growth, Johnson and Mehl (1939) and Avrami (1939) introduced the concept of an extended volume fraction D_x. The factor D_x is defined as the volume fraction of the body transformed disregarding further transformation nucleation in previously transformed material (exclusion), and disregarding the overlap of growing transformation regions (impingement). The extended volume fraction will exceed unity.

The actual transformed volume fraction D of the body is determined from the ratio in the change of the extended and the actual transformed volume fraction, namely,

$$dD/dD_x = 1 - D \,, \tag{3.44}$$

which integrates to,

$$D = 1 - e^{-D_x} \,. \tag{3.45}$$

In the present context the quantities D_x and D will apply to the stress-relieved portion of the stretching ring (Fig. 3.1) during dynamic fracture. The Johnson–Mehl–Avrami (JMA) relation is applicable to two-dimensional bodies or areas, as well as to one-dimensional bodies or lines. Further discussion of the statistical relationship between D and D_x is addressed in Chap. 4.

Although the work of Johnson and Mehl (1939) and Avrami (1939) was focused on phase transformations in materials, their results have more general application. Their result (the JMA relation) is based on the statistics of survival, in this case, survival at any time of the, as yet, untransformed volume. The concept is independent of the physics involved and is applicable to any nucleation and growth process which is random in nature. The JMA relation allows initial attention to focus on the physics of the nucleation and growth process at a single site. Equation (3.45) will then account for the coalescence of multiple transforming regions.

Consequently, analogous to Mott's (3.40), an expression for the number of fractures per unit length which occur at a past time τ within interval $d\tau$, ignoring the stress-released regions, is

$$dN_x = \lambda(\eta)\, d\eta \,. \tag{3.46}$$

In (3.46) $\eta = \dot{\varepsilon}\tau$ is identified as a non-dimensional time or, equivalently, as the strain at past time τ. Release waves from fractures at past time τ (or η) will have propagated a distance,

$$x = g(\varepsilon - \eta) \;, \tag{3.47}$$

at the present time t (or $\varepsilon = \dot{\varepsilon}t$). The function, $g(\varepsilon)$ accounts for either elastic wave speed in elastic fracture or Mott's diffusive wave speed for plastic fracture provided previously in (3.1) and (3.2). Therefore, the increment in extended stress release region due to the earlier fracture is,

$$dD_x = 2g(\varepsilon - \eta)\, dN_x = 2g(\varepsilon - \eta)\, \lambda(\eta)\, d\eta \,, \tag{3.48}$$

where the factor of 2 accounts for right and left facing release waves from each fracture. Integrating over past time to the present yields,

$$D_x = 2\int_0^{\varepsilon} g(\varepsilon - \eta)\, \lambda(\eta)\, d\eta \,. \tag{3.49}$$

Equation (3.45) then provides,

$$D(\varepsilon) = 1 - e^{-D_x(\varepsilon)} \,, \tag{3.50}$$

the fractional stress-relieved region at any time in the dynamic fracture process.

3.6 Fragment Size in the Mott Fracture Process

Perhaps most basic to a dynamic fragmentation event is the characteristic size of the fragments produced. An experiment, such as the rapidly expanding ring shown in Fig. 3.1, results in a number of fragments that can be counted. This number can be divided by the circumferential length of the ring to determine an average fragment length. Additional testing reveals that the number of fractures produced is dependent on both the mechanical properties of the test material as well as the dynamic conditions achieved. This dependence is readily illustrated in Fig. 3.13 in which fragment numbers from similar tests on rapidly expanding aluminum and copper rings are plotted against the radial expansion velocity imparted to the ring at fracture [Grady and Benson, 1983].

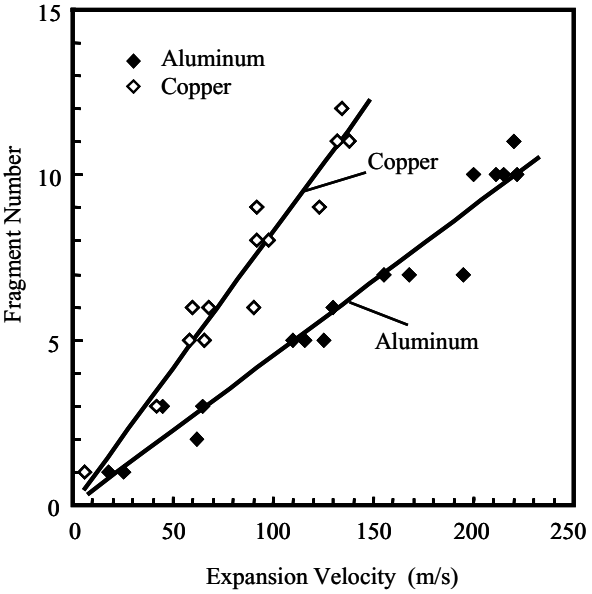

Fig. 3.13. Representative tests showing fragment number versus expansion velocity for fragmenting aluminum and copper ring experiments [Grady and Benson, 1983]

3.6.1 Analysis of Elastic Fracture

In pursuing further the extended statistical approach initiated in the previous section in treating the dynamic fracture model posed by Mott, the power-law fracture frequency function (which results in Weibull extreme value statistics) will be used. Consider first, elastic fracture in which fracture release waves travel at a constant elastic wave velocity. Salient features of the analysis are readily illustrated by the elastic fracture case, while the mathematics are modestly simpler. Accordingly, the power-law fracture frequency from (3.30) and the elastic wave speed (3.2) yield through (3.49),

$$D_x = 2\frac{c}{\dot{\varepsilon}}\frac{n}{\sigma^n}\int_0^{\varepsilon}(\varepsilon-\eta)\,\eta^{n-1}d\eta\,, \tag{3.51}$$

where the elastic wave speed $c=\sqrt{E/\rho}$ has been introduced. The substitution $y=\eta/\varepsilon$ yields,

$$D_x = 2\frac{c}{\dot{\varepsilon}}\frac{n}{\sigma^n}\varepsilon^{n+1}\int_0^{1}(1-y)\,y^{n-1}dy\,, \tag{3.52}$$

where the integral has the solution in terms of the gamma function,

$$\frac{\Gamma(n)\,\Gamma(2)}{\Gamma(n+2)} = \frac{1}{n(n+1)}\,. \tag{3.53}$$

Consequently,

$$D_x = \frac{2c}{(n+1)\,\dot{\varepsilon}\sigma^n}\varepsilon^{n+1}\ , \tag{3.54}$$

and, through (3.50),

$$D = 1 - e^{-\frac{2c}{(n+1)\dot{\varepsilon}\sigma^n}\varepsilon^{n+1}}\ . \tag{3.55}$$

Fracture activation within the unrelieved portion of the stretching body is then calculated through,

$$dN = (1-D)\,\lambda\,(\varepsilon)\,d\varepsilon\ . \tag{3.56}$$

Substituting the appropriate relations, the number of fractures per unit length occurring in the fragmentation process is obtained from the integral over all time,

$$N = \frac{n}{\sigma^n}\int_0^\infty \varepsilon^{n-1}e^{-(a\varepsilon)^{n+1}}d\varepsilon\ , \tag{3.57}$$

where the notation has been simplified through,

$$a^{n+1} = \frac{2c}{(n+1)\,\dot{\varepsilon}\sigma^n}\ . \tag{3.58}$$

Substitute $y = (a\varepsilon)^{n+1}$ in (3.57) yields,

$$N = \frac{1}{(a\sigma)^n}\frac{n}{n+1}\int_0^\infty y^{\frac{n}{n+1}-1}e^{-y}dy\ , \tag{3.59}$$

where the integral is the complete gamma function $\Gamma(n/(n\,+\,1))$. In the original notation, the fracture number per unit length is arrived at,

$$N = \left(\frac{n}{n+1}\right)^{\frac{1}{n+1}}\Gamma\left(\frac{n}{n+1}\right)\left(\frac{\dot{\varepsilon}n}{2c\sigma}\right)^{\frac{n}{n+1}}\ . \tag{3.60}$$

For the special case of $n = 1$,

$$N = \frac{1}{2}\sqrt{\frac{\pi\dot{\varepsilon}}{c\sigma}}\ , \tag{3.61}$$

while for large n approximately,

$$N = \frac{\dot{\varepsilon}n}{2c\sigma}\ . \tag{3.62}$$

3.6.2 Analysis of Plastic Fracture

A solution for the plastic fracture problem considered by Mott follows similar analysis. Using instead the relation for the diffusive propagation of Mott waves (3.1) the expression for the extended fracture release region corresponding to (3.51) becomes,

$$D_x = 2\sqrt{\frac{2Y}{\rho\dot{\varepsilon}^2}}\frac{n}{\sigma^n}\int_0^{\varepsilon}(\varepsilon-\eta)^{1/2}\eta^{n-1}d\eta\ , \tag{3.63}$$

or with $y = \eta/\varepsilon$,

$$D_x = 2\sqrt{\frac{2Y}{\rho\dot{\varepsilon}^2}}\frac{n}{\sigma^n}\varepsilon^{n+1/2}\int_0^{1}(1-y)^{1/2}y^{n-1}dy\ . \tag{3.64}$$

Solving for the integral,

$$\frac{\sqrt{\pi}}{2n+1}\frac{\Gamma(n)}{\Gamma(n+1/2)}\ , \tag{3.65}$$

yields,

$$D_x = \sqrt{\pi}\frac{n}{n+1/2}\frac{\Gamma(n)}{\Gamma(n+1/2)}\sqrt{\frac{2Y}{\rho\dot{\varepsilon}^2}}\frac{\varepsilon^{n+1/2}}{\sigma^n}\ . \tag{3.66}$$

The total number of fractures is calculated similarly through the simplification,

$$D_x = (a\varepsilon)^{n+1/2}\ , \tag{3.67}$$

leading to the integral expression for the fragment number,

$$N = \frac{1}{(a\sigma)^n}\frac{n}{n+1/2}\int_0^{\infty} y^{\frac{n}{n+1/2}-1}e^{-y}dy\ , \tag{3.68}$$

and yielding,

$$N = \frac{1}{(a\sigma)^n}\frac{n}{n+1/2}\Gamma\left(\frac{n}{n+1/2}\right)\ . \tag{3.69}$$

The fragment number per unit length in the original notation for plastic fracture in the Mott model becomes,

$$N = \beta_n\left(\frac{\rho\dot{\varepsilon}^2}{2\pi Y}\frac{n}{\sigma}\right)^{\frac{n}{2n+1}}\ , \tag{3.70}$$

where,

$$\beta_n = \left(\frac{2n}{2n+1}\right)^{\frac{1}{2n+1}}\left(\frac{1}{\sqrt{n}}\frac{\Gamma(n+1/2)}{\Gamma(n)}\right)^{\frac{2n}{2n+1}}\Gamma\left(\frac{2n}{2n+1}\right)\ . \tag{3.71}$$

Again the special cases yield for $n = 1$,

$$N = \Gamma\left(\frac{2}{3}\right)\left(\frac{\rho\dot{\varepsilon}^2}{12Y\sigma}\right)^{1/3} , \tag{3.72}$$

while for large n approximately,

$$N = \sqrt{\frac{\rho\dot{\varepsilon}^2}{2\pi Y}\frac{n}{\sigma}} . \tag{3.73}$$

Comparing standard deviation for the power-law fracture frequency ($\simeq 1.28\sigma/n$) with that for extreme-value function explored by Mott ($\simeq 1.28/\gamma$) we find from (3.73) that an average fragment length of $1/N$ gives,

$$\sqrt{\pi}\sqrt{\frac{2Y}{\rho\dot{\varepsilon}^2}\frac{\sigma}{n}} = \sqrt{\pi}L_o , \tag{3.74}$$

where L_o is the same distribution length scale determined by Mott ((3.43) and Fig. 3.11). Mott determined graphically that an average fragment length was approximately 1.5 L_o, close indeed to the analytic result in (3.74).

3.6.3 Analysis with the Mott Fracture Hazard Function

The same analysis can be carried through with the strain-to-fracture activation function assumed by Mott, namely, the Gumbel extreme value distribution provided by (3.37) and displayed in Fig. 3.10. Using the release propagation function,

$$g(\varepsilon - \eta) = \sqrt{\frac{2Y}{\rho\dot{\varepsilon}^2}}(\varepsilon - \eta)^{1/2} , \tag{3.75}$$

and the activation function,

$$\lambda(\eta) = \frac{1}{\sigma}e^{(\eta-\mu)/\sigma} , \tag{3.76}$$

the extended fracture release region corresponding to (3.63) becomes,

$$D_x = \frac{2}{\sigma}\sqrt{\frac{2Y}{\rho\dot{\varepsilon}^2}}\int_0^{\varepsilon}(\varepsilon - \eta)^{1/2}e^{(\eta-\mu)/\sigma}d\eta . \tag{3.77}$$

The Gumbel distribution has the awkward feature of providing finite values for negative ε. For realistic values of σ and μ, however, this contribution is vanishing small and the integral in (3.77) over the interval $[-\infty, \varepsilon]$ can be assumed providing, after the substitution $y = \varepsilon - \eta$,

$$D_x = \frac{2}{\sigma}\sqrt{\frac{2Y}{\rho\dot{\varepsilon}^2}}e^{(\varepsilon-\mu)/\sigma}\int_0^\infty y^{1/2}e^{-y/\sigma}dy\ , \tag{3.78}$$

or,

$$D_x = 2\Gamma\left(2/3\right)\sqrt{\frac{2Y\sigma}{\rho\dot{\varepsilon}^2}}e^{(\varepsilon-\mu)/\sigma}\ . \tag{3.79}$$

Using the relation between D and D_x from (3.45) and,

$$N = \int_0^\infty (1-D)\lambda\left(\varepsilon\right)d\varepsilon\ ,$$

results in,

$$N = \frac{1}{\sigma}\int_0^\infty e^{(\varepsilon-\mu)/\sigma}e^{-be^{(\varepsilon-\mu)/\sigma}}d\varepsilon\ , \tag{3.80}$$

where b is the pre-exponential term in (3.79). The substitution $y = \exp(\varepsilon-\eta)/\sigma$, and recognizing that the lower limit is approximately zero for $\mu/\sigma \gg 1$, yields,

$$N = \frac{1}{\sqrt{\pi}}\sqrt{\frac{\rho\dot{\varepsilon}^2}{2Y\sigma}}\ . \tag{3.81}$$

Accounting for the differing definitions of σ in the power-law and exponential hazard functions, (3.81) and (3.73) are identical. Recall that Mott used $\gamma = 1/\sigma$ in his application of the Gumbel distribution.

Again, it is emphasized that the lack of a shape parameter in the Gumbel extreme value distribution leads to a unique first power dependence of fragment number on strain rate (3.81). In contrast, strain rate dependence based on the Weibull extreme value statistics depends on the distribution shape parameter n (3.70).

3.7 Size Distribution in the Mott Fracture Process

The statistical analysis developed in the last several sections can be further pursued to provide analytic solutions for the distributions in fragment size. These analytic distribution solutions correspond to the graphic distribution determined in the original analysis of Mott shown in Fig. 3.11. The solution method is somewhat more detailed in that it is necessary to assess statistically when fracture release waves initiate and when they arrest, thus determining the unbroken distance spanned by the wave. The process is illustrated in Fig. 3.14 in which release waves originating from two separate fractures propagate distances l_1 and l_2, respectively, before colliding and arresting. The

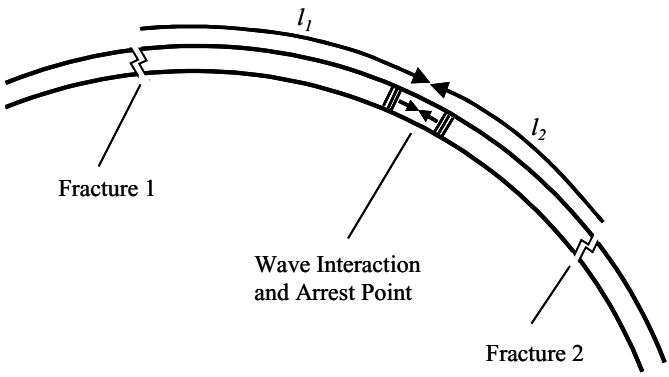

Fig. 3.14. Release waves originating from fracture 1 and fracture 2 travel distances l_1 and l_2, respectively, before arresting. The distance $l_1 + l_2$ constitutes the length of one fragment

distance, $l_1 + l_2$ constitutes the length of one fragment. The statistical fragment size distribution is then the probability function for the expectation of fragments of this specified length.

The solution is carried out for both elastic and plastic (Mott) fracture in the present subsection. The solution method is also presented in general terms in a later chapter, providing a clearer display of the solution methodology.

3.7.1 Analysis of Elastic Fracture

The solution will again be pursued first for that of elastic fracture in which fracture release waves travel at the constant speed $c = \sqrt{E/\rho}$. Also a power-law fracture frequency expression continues to be assumed. The analysis will start with the solution for the extended length fraction of stress relieved region from (3.54),

$$D_x = \frac{2c}{(n+1)\,\dot{\varepsilon}\sigma^n}\varepsilon^{n+1} = (a\varepsilon)^{n+1} \quad , \tag{3.82}$$

where,

$$D = 1 - e^{-D_x} = 1 - e^{-(a\varepsilon)^{n+1}} \quad . \tag{3.83}$$

Calculate first the number of activated release waves N_x without regard for exclusion (activation within previous stress relieved region) or impingement (collision and arrest of opposing release waves). The symbols N_x and N refer here to the number of Mott waves and not the number of fractures as in previous sections. The rate of activation of release waves I_x is,

$$I_x = 2\lambda\,(\varepsilon) = 2\frac{n}{\sigma}\left(\frac{\varepsilon}{\sigma}\right)^{n-1} \quad , \tag{3.84}$$

where the factor of 2 accounts for both a right and left facing wave emanating from each fracture point. N_x is then simply,

$$N_x = \int_0^{\varepsilon} I_x d\varepsilon = 2\left(\frac{\varepsilon}{\sigma}\right)^n . \tag{3.85}$$

But at any time (or strain) a fraction D of the length of the body has been stress relieved. The actual number of active release waves is,

$$N = N_x\,(1-D) = 2\left(\frac{\varepsilon}{\sigma}\right)^n e^{-(a\varepsilon)^{n+1}} , \tag{3.86}$$

accounting for both exclusion and impingement.

The rate of change of N is then,

$$\frac{dN}{d\varepsilon} = \frac{2n}{\sigma^n}\varepsilon^{n-1}e^{-(a\varepsilon)^{n+1}} - \frac{2\,(n+1)\,a^{n+1}}{\sigma^n}\varepsilon^{2n}e^{-(a\varepsilon)^{n+1}} . \tag{3.87}$$

From (3.87) we identify the rate of activation of release waves,

$$I^+ = \frac{2n}{\sigma^n}\varepsilon^{n-1}e^{-(ae)^{n+1}} , \tag{3.88}$$

and the rate of arrest of release waves,

$$I^- = -\frac{2\,(n+1)\,a^{n+1}}{\sigma^n}\varepsilon^{2n}e^{-(a\varepsilon)^{n+1}} . \tag{3.89}$$

The activation rate I^+ can also be calculated from the extended activation rate I_x by accounting for exclusion,

$$I^+ = I_x\,(1-D) = \frac{2n}{\sigma^n}\varepsilon^{n-1}e^{-(a\varepsilon)^{n+1}} . \tag{3.90}$$

Also, note that the arrest rate may be written,

$$I^- = -\,(n+1)\,a^{n+1}\varepsilon^n N . \tag{3.91}$$

With the above relations, we will now proceed to calculate the number of waves which activated at an earlier time η and arrested at a later time ε. The unbroken distance l spanned by these waves will all be the same (Fig. 3.14).

Accordingly, the number δN of release waves activated at time η within increment $\delta\eta$ is, from (3.88),

$$\delta N = \frac{2n}{\sigma^n}\eta^{n-1}e^{-(a\eta)^{n+1}}\delta\eta . \tag{3.92}$$

The fraction of δN arrested at later time ε is, from (3.91),

$$d\,(\delta N) = -\,(n+1)\,a^{n+1}\varepsilon^n\,(\delta N)\,d\varepsilon . \tag{3.93}$$

Equation (3.93) can be separated and integrated to obtain,

$$\delta N = Ae^{-(a\varepsilon)^{n+1}} \ , \tag{3.94}$$

where A is a constant of integration. Setting ε equal to the early time η in (3.94) the constant of integration is seen from (3.92) to be,

$$A = \frac{2n}{\sigma^n}\eta^{n-1}\delta\eta \ , \tag{3.95}$$

and consequently, (3.94) becomes,

$$\delta N = \frac{2n}{\sigma^n}\eta^{n-1}e^{-(a\varepsilon)^{n+1}}\delta\eta \ . \tag{3.96}$$

Substituting the results of (3.96) into the right side of (3.93) yields,

$$d\left(\delta N\right) = -\frac{2n\left(n+1\right)a^{n+1}}{\sigma^n}\varepsilon^n\eta^{n-1}e^{-(a\varepsilon)^{n+1}}\delta\eta d\varepsilon \ . \tag{3.97}$$

We now make the variable change,

$$x = \frac{c}{\dot{\varepsilon}}\left(\varepsilon - \eta\right) \ , \tag{3.98}$$

where x is the distance traveled by the release wave over the time interval $\varepsilon - \eta$.

At the same time switching the incremental order on the left hand side (3.97) results in,

$$\delta\left(dN\right) = -\frac{2n\left(n+1\right)a^{n+1}}{\sigma^n}\frac{\dot{\varepsilon}}{c}dx\left(\eta + \frac{\dot{\varepsilon}}{c}x\right)^n \eta^{n-1}e^{-a^{n+1}\left(\eta+\frac{\dot{\varepsilon}}{c}x\right)^{n+1}}\delta\eta \ . \tag{3.99}$$

Integrating over all past time η provides,

$$dN = -\frac{2n\left(n+1\right)a^{n+1}}{\sigma^n}\frac{\dot{\varepsilon}}{c}dx\int_0^\infty\left(\eta + \frac{\dot{\varepsilon}}{c}x\right)^n \eta^{n-1}e^{-a^{n+1}\left(\eta+\frac{\dot{\varepsilon}}{c}x\right)^{n+1}}\delta\eta \ . \tag{3.100}$$

Substituting y for the exponential exponent simplifies the integral to,

$$\frac{dN}{dx} = -\frac{2n}{\sigma^n}\frac{\dot{\varepsilon}}{c}\left(\frac{\dot{\varepsilon}x}{c}\right)^{n-1}\int_b^\infty\left[\left(y/b\right)^{1/(n+1)} - 1\right]^{n-1}e^{-y}dy \ , \tag{3.101}$$

where,

$$b = \frac{2}{n+1}\left(\frac{\dot{\varepsilon}}{c\sigma}\right)^n x^{n+1} \ . \tag{3.102}$$

Equation (3.101), when normalized, provides the probability distribution in lengths of unbroken release wave segments, such as l_1 and l_2 in Fig. 3.14. It does not, however, provide the distribution in fragment length as release wave

segments combined in pairs to constitute fragments (i.e., l_1 and l_2 in Fig. 3.14 combine to make a fragment of length, $l = l_1 + l_2$).

Thus, the distribution in fragment lengths is,

$$f(l)\,dl = \int\limits_{l=l_1+l_2} p(l_1)\,p(l_2)\,dl_i dl_2 \;, \tag{3.103}$$

where $p(l_i)$ is the normalized distribution in release wave segments and the integral is over all release wave segment length l_1 and l_2 which sum to l.

Equation (3.101) is not analytically tractable for arbitrary values of n. It is readily solved for $n = 1$, however, and this solution is provided here. Recall that $n = 1$ corresponds to a statistically uniform rate of fracture activation following onset of the first fracture. For $n = 1$ (3.101) reduces to,

$$\frac{dN}{dx} = -\frac{2}{\sigma}\frac{\dot{\varepsilon}}{c}\int\limits_{b}^{\infty} e^{-y}dy \;, \tag{3.104}$$

or,

$$\frac{dN}{dx} = \frac{2\dot{\varepsilon}}{\sigma c}e^{-\frac{\dot{\varepsilon}}{\sigma c}x^2} \;. \tag{3.105}$$

Integrating (3.105) provides the normalizing factor and the probability distribution in release wave segments,

$$p(x) = 2\sqrt{\frac{\dot{\varepsilon}}{\pi\sigma c}}e^{-\frac{\dot{\varepsilon}}{\sigma c}x^2} \;. \tag{3.106}$$

or, after introducing a length scale,

$$l_o = \sqrt{\frac{2\sigma c}{\dot{\varepsilon}}} \;, \tag{3.107}$$

Equation (3.103) provides the integral,

$$f(l)\,dl = \frac{8}{\pi l_o^2}\int\limits_{l=l_1+l_2} e^{-2\left(l_1^2+l_2^2\right)/l_o^2}dl_1 dl_2 \;. \tag{3.108}$$

The integral is completed through,

$$l = l_1 + l_2,\; \xi = l_1 - l_2,$$

$$dl_1 dl_2 = \left[\partial(l_1, l_2)/\partial(l, \xi)\right] dl d\xi \;,$$

yielding,

$$f(l) = \frac{4}{\pi l_o^2}e^{-(l/l_o)^2}\int\limits_{-l}^{l} e^{-(\xi/l_o)^2}d\xi \;, \tag{3.109}$$

and finally,

$$f(l) = \frac{4}{\sqrt{\pi}} \frac{1}{l_o} e^{-(l/l_o)^2} \operatorname{erf}(l/l_o) \ , \tag{3.110}$$

where erf( ) is the error function. The cumulative distribution is provided by,

$$F(l) = \int_0^l f(l)\, dl \ , \tag{3.111}$$

while the expected value of l is,

$$\langle l \rangle = \int_0^\infty l f(l) dl = \sqrt{\frac{2}{\pi}} l_o \ , \tag{3.112}$$

identically equal to $\langle l \rangle = 1/N$ for the predicted fragment number per unit length from (3.61). Both the probability density and complementary cumulative distributions for fragment length based on elastic fracture are shown in Fig. 3.15.

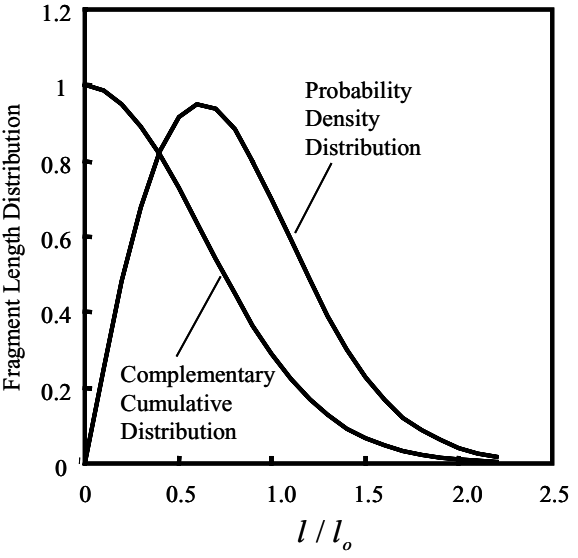

Fig. 3.15. Calculated probability density and complementary cumulative distributions in fragment lengths based on the Mott theoretical model for elastic fracture

3.7.2 Analysis of Plastic Fracture

The similar solution for the plastic fracture process pursued by Mott follows identical steps. A plastic wave speed, $c = \sqrt{2Y/\rho}$, introduced into the

relation for the diffusive propagation of Mott waves yields (3.66) for the extended length fraction of stress-relieved region. Assuming as before, a power-law relation for the rate of fracture activation, the probability distribution in lengths of unbroken release wave segments corresponding to (3.101) is,

$$\frac{1}{x}\frac{dN}{dx} = -\frac{4n}{\sigma^n}\left(\frac{\dot{\varepsilon}}{c}\right)^2\left(\frac{\dot{\varepsilon}x}{c}\right)^{2(n-1)}\int_b^\infty\left[(y/b)^{2/(2n+1)}-1\right]^{n-1}e^{-y}dy\ , \quad (3.113)$$

where,

$$b = \frac{2\sqrt{\pi}n}{2n+1}\frac{\Gamma(n)}{\Gamma(n+1/2)}\left(\frac{\dot{\varepsilon}}{c}\right)^{2n}\frac{x^{2n+1}}{\sigma^n}\ . \quad (3.114)$$

As before, the analytic solution cannot be pursued further for arbitrary values of n. For the special case of $n = 1$ (3.113) reduces to,

$$\frac{1}{x}\frac{dN}{dx} = -\frac{4}{\sigma}\left(\frac{\dot{\varepsilon}}{c}\right)^2\int_b^\infty e^{-y}dy\ , \quad (3.115)$$

with,

$$b = \frac{4}{3}\sigma\left(\frac{\dot{\varepsilon}}{c}\right)^2 x^3\ , \quad (3.116)$$

yielding,

$$\frac{dN}{dx} = \frac{4}{\sigma}\left(\frac{\dot{\varepsilon}}{c}\right)^2 xe^{-\frac{4}{3}\frac{1}{\sigma}\left(\frac{\dot{\varepsilon}}{c}\right)^2 x^3}\ . \quad (3.117)$$

Introducing the length scale,

$$l_o = \left(\frac{3\sigma}{4}\left(\frac{c}{\dot{\varepsilon}}\right)^2\right)^{1/3}\ , \quad (3.118)$$

and normalizing, (3.117) leads to,

$$p(x) = \beta\frac{x}{l_o^2}e^{-(x/l_o)^3}dx\ , \quad (3.119)$$

for the probability density distribution of segment lengths corresponding to (3.106) for elastic fracture and where $\beta = 3/\Gamma(2/3)$.

Combining segment lengths in pairs as discussed in the paragraphs leading to (3.103) provides the fragment size distribution for plastic fracture,

$$f(l) = \frac{\beta^2}{4}\frac{1}{l_o}\left(\frac{l}{l_o}\right)^3 e^{-\frac{1}{4}(l/l_o)^3}\int_0^1\left(1-y^2\right)e^{-\frac{3}{4}(l/l_o)^3y^2}dy\ . \quad (3.120)$$

The integral in (3.120) can be manipulated into an error function expression if desired, although, it is readily computed with most available math software.

The expected fragment size is calculated from the integral,

$$\langle s \rangle = \int_0^\infty l f(l)\, dl \ . \tag{3.121}$$

Performed numerically the integral yields $\langle s \rangle \simeq 1.48 l_o$ with l_o provided from (3.118). This calculation agrees, as it should, with the previous calculation for the total fragment number per unit length in (3.72).

It is also of interest to compare the present analytic distribution with that generated graphically by Mott (1947). Comparisons for both probability density and complementary cumulative probability distributions are shown in Fig. 3.16. Recall, however, that the assumed laws governing the statistical fracture frequency differ markedly in the two calculations. Mott assumed an exponentially escalating rate of fracture activation (3.31). A power law fracture frequency (3.30) was assumed in the analytic derivation which, for the sake of analytic tractability, was reduced to a uniform rate of fracture activation (3.29) corresponding to $n = 1$ in the power law expression. Influence of the differing fracture frequency laws on the statistical distribution in fragment lengths is not known.

Mott's graphical distribution and the present analytic distribution agree quite well as the comparison in Fig. 3.16 shows. Modest differences are perhaps best revealed in the comparison of the complementary cumulative distributions. The present distribution for plastic fracture differs from that of elastic fracture as comparison with the plot in Fig. 3.17 reveals. The comparisons indicate that the law governing the propagation of release waves from the point of fracture (diffusive Mott waves versus elastic waves) is the first order effect in governing the distribution shape. The fracture frequency law, on the other hand, appears to have a smaller influence on the shape of the distribution.

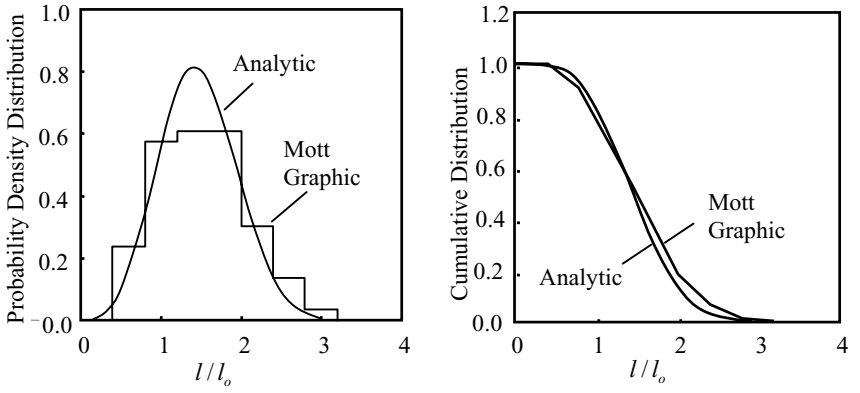

Fig. 3.16. Comparison of the present analytic distribution in fragment lengths for plastic fracture with the graphical distribution of Mott

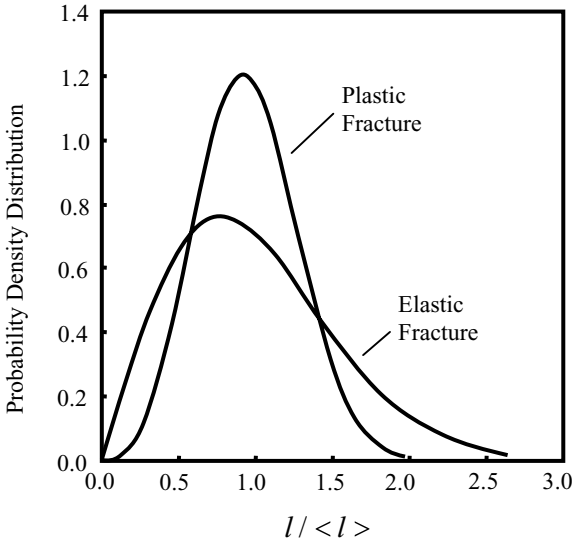

Fig. 3.17. Analytic length distributions for models of elastic and plastic fracture based on Mott statistical fragmentation

The normalizing length scale l_o for the two distributions in Fig. 3.16 are,

$$l_o = \sqrt{2Y/\rho\dot{\varepsilon}^2\gamma}\,,$$

from the Mott (1947) analysis and,

$$l_o = \left[(3\sigma/4)\left(2Y/\rho\dot{\varepsilon}^2\right)\right]^{1/3}\,,$$

from the analytic solution. The separate derivations are based on markedly different assumed fracture frequency laws. That the two distributions successfully overlay without adjustment of the independent length scales seems remarkable.

References

Avrami, M. (1939) *J. Chem. Phys.*, 7, 1103.

Barenblatt (1962), *Adv. Appl. Mech.* 7, 55.

Doremus, R. H. (1983), Fracture Statistics: A Comparison of the Normal, Weibull and Type I Extreme Value Distributions, *J. Appl. Phys.*, 54, 193–198.

Dugdale (1960), *J. Mech. Phys. Solids*, 8, 100.

Grady, D. E. and Benson, D. A. (1983), Fragmentation of Metal Rings by Electromagnetic Loading, *Experimental Mechanics* 23 (4), 393–400.

Grady, D. E., Kipp, M. E. and Benson, D. A. (1984), Energy and Statistical Effects in the Dynamic Fragmentation of Metal Rings, *Proceedings of the Conference of the Mechanical Properties of High Rates of Strain*, Oxford, 1984, Inst. Phys. Conf. Ser. No. 70, 315–320.

Hahn, G. J. and Shapiro, S. S. (1967), *Statistical Models in Engineering*, John Wiley & Sons, New York.

Johnson, W. A. and Mehl, R. F. (1939), Reaction Kinetics in Processes of Nucleation and Growth, *Trans. AIMME*, 135, 414–458.

Kipp, M. E. and Grady, D. E. (1985), Dynamic Fracture Growth and Interaction in One Dimension, *J. Mech. Phys. Solids* 33 (4), 399–415.

Lee, E. H. (1967), The Continuum Mechanics Aspect of Material Properties Determination, *Energetics III*, W. Mueller and M. Shaw, eds., pp. 85–122, Gordon and Breach, New York.

Matthews, J. and Walker, R. L. (1964), *Mathematical Methods of Physics*, W. A. Benjamin, Inc., New York, pp. 228–234.

Mott, N. F. (1947), Fragmentation of Shell Cases, *Proc. Royal Soc.*, A189, 300–308, January.

Wesenberg, D. L. and Sagartz, M. J. (1977), Dynamic Fracture of 6061-T6 Aluminum Cylinders, *J. Appl. Mech.*, 44, 643–646.